

A compressed wide period-tunable grating working at low voltage*

Liu Xiang(刘翔)^{1,2}, Li Tie(李铁)^{1,†}, Ming Anjie(明安杰)¹, and Wang Yuelin(王跃林)¹

(1 State Key Laboratory of Transducer Technology, National Key Laboratory of Microsystem Technology, Shanghai Institute of Microsystems and Information Technology, Chinese Academy of Sciences, Shanghai 200050, China)

(2 Graduate University of the Chinese Academy of Sciences, Beijing 100049, China)

Abstract: A MEMS compressed period-tunable grating device with a wide tuning range has been designed, fabricated and characterized. To increase the tuning range, avoid instability with tuning and improve the performance, we propose in this paper a period-tunable grating which is compressed by large-displacement comb actuators with tilted folded beams. The experimental results show that the designed grating device has a compression range of up to 144 μm within 37 V driving voltage. The period of the grating can be adjusted continuously from 16 to 14 μm with a tuning range of 12.5%. The maximum tuning range of the first-order diffraction angle is 0.34° at 632.8 nm and the reflectivity of the grating is more than 92.6% in the mid-infrared region. The grating device can be fabricated by simple processes and finds applications in mid-infrared spectrometers.

Key words: period-tunable grating; compressed structure; comb-drive actuator; MEMS

DOI: 10.1088/1674-4926/31/10/104010

EEACC: 4145; 2575

1. Introduction

The grating is an important diffractive device and a high-precision period structure is required for good performance. Compared with traditional gratings having low precision, fixed period and large volume, the tunable grating, based on MEMS technology, has the advantages of high precision, flexibility and compactness with low cost and excellent performance. It has become more popular in recent years due to its promising applications in displays, spectrometers, external cavity lasers, programmable masks and optical telecommunications^[1,2], etc.

In the last decade, MEMS tunable gratings, including phase-tunable^[2], incident-angle-tunable^[3] and period-tunable gratings^[4–8], have been extensively studied. Some researches have given rise to applications in commercial products^[2]. Among phase-tunable and incident-angle-tunable gratings, the period-tunable grating is distinguished by its relatively simple structure and large tuning ratio, which favors mass production by simple fabrication processes, and good performance.

In previous works^[4–8], period-tunable gratings using piezoelectric, thermal or comb actuators have been studied, and their tuning ranges were usually small. A comb driver with a small (3%) tuning range under 100 V driving voltage was adopted by Tormen^[6]. Other researchers used elastomer actuators to drive the grating with a periodicity tuning of 7.5%^[7], but their driving voltage was as high as several thousand volts. Recently, Yang^[8] reported a grating with a tuning ratio of 25% under 19 V using a thermal actuator; while its response time and actuation speed was slow, compared with an electrostatic actuator, the power consumption was high.

The period-tunable gratings reported previously^[4–8] were all based on stretched structures. According to grating theory, the period is the most critical parameter for a grating device, and a small period can enlarge the diffraction angle and im-

prove the grating diffraction efficiency and resolution. A compressed structure decreases the period with tuning and leads to the advancement of performance. Furthermore, as the initial period need not be very small, it would be helpful in achieving high performance and yield, with a simple fabrication process.

In this paper, the developed comb actuators are designed to compress the grating. Eight comb actuators are adopted to increase the actuating force and decrease the working voltage. Tilted folded beams and comb actuators with non-initial comb overlap and linearly engaging comb fingers are employed to improve the side stability. A period-tunable grating with a wide tuning range and a continuously adjusting function is designed and fabricated.

2. Design

The electrostatic actuator is a device which has been widely used in MEMS devices owing to its large displacement, strong driving force and high speed. In particular, the comb driver has always been popular in MEMS since it was invented by Tang^[9]. In this paper, the grating is compressed by the developed comb actuators since the compressed structure can improve the performance and simplify the fabrication process. We have designed the device based on two important rules to achieve a high performance grating with a large tuning range. Firstly, the optimized comb drivers are designed to increase the driving displacement under a low working voltage. Secondly, tilted folded beams, grating support beams and the developed comb drivers are introduced to improve the stability of the device.

Figure 1 shows a schematic of the MEMS tunable grating. The device is mainly composed of grating slats and eight comb-drive actuators. In the device, the anchors and the support frame are fixed by bonding to a glass substrate; the grating, the tilted folded beams and the comb drivers can move under the applied

* Project supported by the State Key Development Program for Basic Research of China (No. 2006CB30040).

† Corresponding author. Email: tli@mail.sim.ac.cn

Received 15 March 2010, revised manuscript received 4 June 2010

© 2010 Chinese Institute of Electronics

Table 1. Detailed dimensions of the period-tunable MEMS grating.

Number of gratings	71	Number of finger pairs	180 × 8
Length of grating	1000 μm	Width of comb finger	4.5 μm
Width of grating	8.5 μm	Gap of comb finger	2.5 μm
Gap of grating	7.5 μm	Length of tilted folded beam	1200 μm
Length of spring flexures	150 μm	Width of tilted folded beam	5.8 μm
Width of spring flexures	2.5 μm	Grating area	1.15 mm × 1 mm
Structure thickness	50 μm	Dimension of the chip	6 mm × 3.5 mm

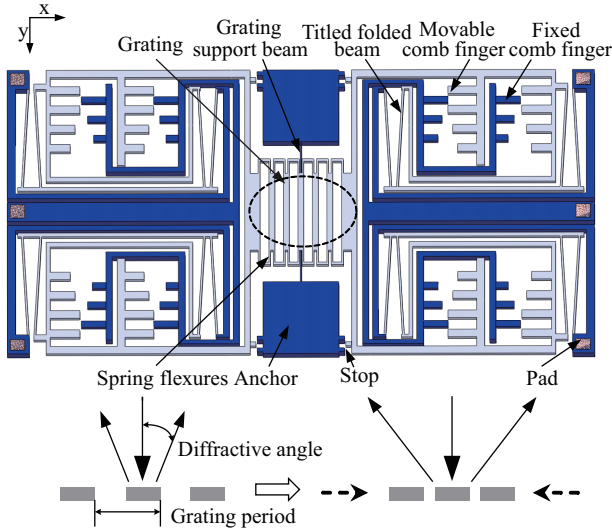


Fig. 1. Schematic diagram of the period-tunable MEMS grating.

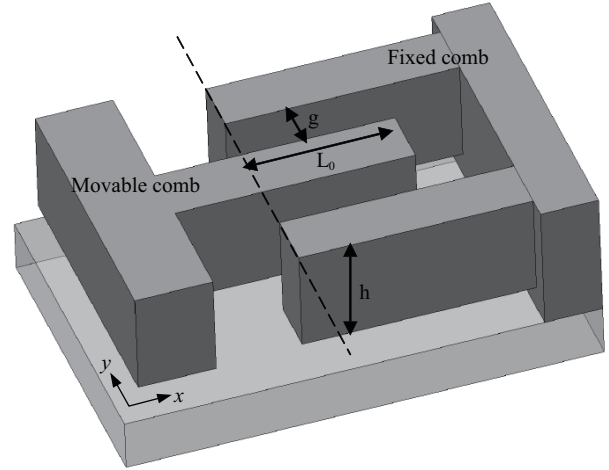


Fig. 2. Cell of engaged comb finger arrays.

voltage. Table 1 shows the dimensions of the proposed period-tunable MEMS grating.

2.1. Design of comb driver

The design of the comb driver in this paper is based on the previous works^[10–12] on the comb actuator for large displacement. A pair of comb fingers is shown schematically in Fig. 2. When a driving voltage is applied between the movable and fixed finger, ignoring edge effects (fringing), the driving force from the electrostatic force in the lateral direction is given by

$$F_x = \frac{1}{2} \frac{dC}{dx} V^2 = \frac{n\epsilon h V^2}{2} \left(\frac{1}{g-y} + \frac{1}{g+y} \right). \quad (1)$$

Besides the electrostatic force along the x -axis, there is an electrostatic force pulling the movable comb and fixed comb together. The electrostatic force in the y -direction is:

$$F_{ey} = \frac{1}{2} \frac{dC}{dy} V^2 = \frac{n\epsilon h(L_0+x)V^2}{2(g-y)^2} - \frac{n\epsilon h(L_0+x)V^2}{2(g+y)^2}, \quad (2)$$

where C is the capacitance between the parallel-plate comb, V is the applied voltage, n is the number of comb finger pairs, ϵ is the dielectric constant of air, h is the height of comb finger, g is the comb gap between fingers, L_0 is the overlapping comb length, and x, y are the comb displacement in the x -direction and y -direction respectively.

Equation (1) shows that the driving force is directly proportional to the number of comb fingers and inversely proportional to the comb gap, so more comb fingers and a small comb gap are adopted to increase the actuating force and decrease the working voltage. Eight comb drivers, instead of two, are used to multiply the lateral driving force.

The overlapping comb area increases with lateral displacement and this leads to large y -axis forces that cause the finger to suddenly snap over sideways. Therefore the comb drivers are unstable when the lateral displacement is large. It is well known that reducing the overlapping area of comb fingers can improve the stability^[11, 12]. There are two ways to achieve this: reduce the initial overlapping lengths of the comb fingers and adjust the lengths of the individual comb fingers. Here, non-initial comb overlap and linearly engaging comb fingers are employed. From our previous work^[12], it was found that these can decrease the longitudinal electrostatic force and improve the side stability without increasing the driving voltage of the maximum displacement. In addition, the compact structure is designed, as shown in Fig. 1, to reduce the device area.

The stiffness of the of the folded suspension beam in the x -direction is given by^[11]

$$k_{x,fb} = \frac{E h_{fb} b_{fb}^3}{L_{fb}^3}, \quad (3)$$

where E is the Young's modulus of silicon, h_{fb}, b_{fb}, L_{fb} are the height, width and length of the folded suspension beam respectively. The stiffness of the spring flexure between two adjacent grating slats (one grating period) in the x -direction is estimated by^[5]

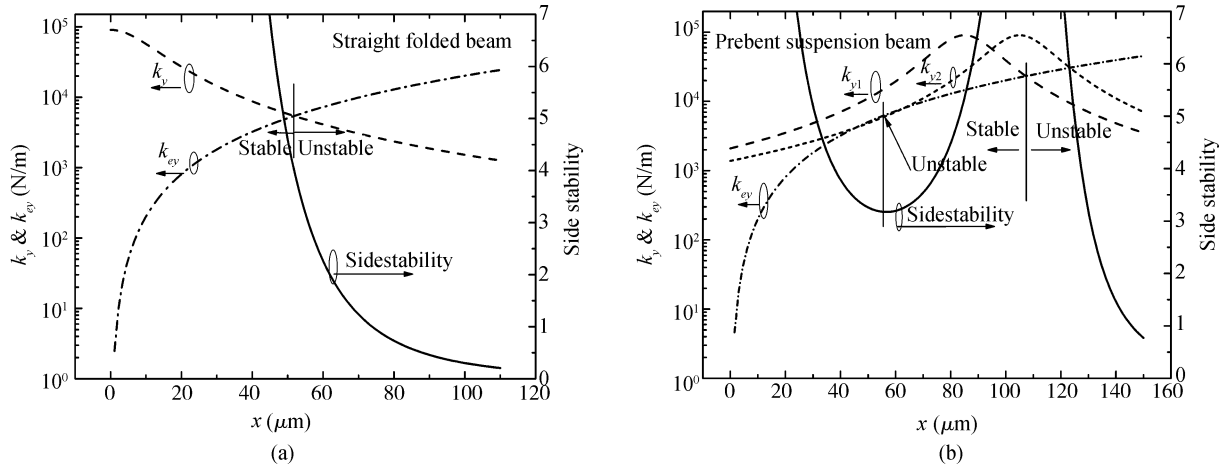


Fig. 3. Relationship of stiffness versus displacement for (a) the straight folded beam and (b) the tilted folded beam with pre-bent length of $x_{pb,1} = 50 \mu\text{m}$ and $x_{pb,2} = 60 \mu\text{m}$.

$$k_{x,sf} = \frac{E h_{sf} b_{sf}^3}{L_{sf}^3}, \quad (4)$$

where h_{sf} , b_{sf} , L_{sf} are the height, width and length of the spring flexure respectively. In static equilibrium the forward electrostatic force is balanced by the restoring force of the folded suspension beams and spring flexures. Then the displacement of the whole grating device is estimated by

$$x = 2 \times \frac{4F_x}{2k_{x,fb} + \frac{2k_{x,sf}}{N+1}} = \frac{4n\varepsilon V^2}{gE} \left[\left(\frac{b_{fb}}{L_{fb}} \right)^3 + \frac{1}{N+1} \left(\frac{b_{sf}}{L_{sf}} \right)^3 \right]^{-1}, \quad (5)$$

where N is the number of grating slats.

2.2. Design of the tilted folded beam

Compared with a straight folded beam, the tilted folded beam can provide better stability^[13, 14], especially when the displacement is large. We define $k_{y,fb}$ to be the side spring stiffness of the folded suspension beam. It is actually a combination of the axial stiffness of the individual suspension beam and the geometric stiffness of the suspension^[11], which is given by

$$k_{y,fb} = \frac{8E h_{fb} b_{fb}^3}{3L_{fb}(x - x_{pb})^2 + 8L_{fb} b_{fb}^2}, \quad (6)$$

where x_{pb} is the pre-bent length of the tilted folded beam. Equation (6) shows that the side spring stiffness decreases with the square of the forward displacement, and therefore the elastic restoring force also decreases with the displacement. It is found that the suspension beam with pre-bent can enlarge the spring stiffness. k_{ey} is the equivalent “negative” spring stiffness of the electrostatic force, which is given by

$$k_{ey} = \left. \frac{\partial F_{ey}}{\partial y} \right|_{y=\delta y} = \frac{2n\varepsilon h V^2 (L_0 + x)}{g^3}. \quad (7)$$

The side stability is the ratio of elastic restoring force to the electrostatic force in the longitudinal direction, which represents the degree of side stability of the actuator. The side stability is given by

$$S = \frac{k_{y,fb}(g^2 - \delta_y^2)^2}{2k_{x,fb}(L_0 + x)^2(g^2 + 3\delta_y^2)}. \quad (8)$$

For stability, $k_{y,fb}$ must be greater than k_{ey} , otherwise the comb drivers become unstable and lead to side sticking of the movable comb and fixed comb finger. Also, the side stability should be larger than 3.5^[12] considering the process tolerance throughout the full movement in the lateral direction.

Figure 3 shows the stiffness of the folded suspension beam and the side stability with the forward displacement. From Fig. 3, it can be seen that the tilted folded beam greatly improves the stability. The comb actuator with the tilted folded beam has good stability even when the displacement is 100 μm , while the maximum stable displacement is 50 μm with the straight beam.

The profile of the tilted folded beam, $w(y)$, is defined by the following equation^[12]:

$$w(y) = c \left(\frac{L_{fb} y^2}{2} - \frac{y^3}{3} \right), \quad (9)$$

where $c = F/2EI$, F is the driving force of the maximum displacement, and $I = b_{fb} h_{fb}^3/12$ is the moment of inertia of the folded beam.

2.3. Design of the compressed structure

The introduction of a compressed structure into tunable gratings has two important advantages. Firstly, it will promote the performance of the grating device. According to grating theory, the period is the key parameter of the grating device. The grating equation indicates that the diffractive angle and angular dispersion increase as the period decreases. The resolving power is given by

$$R = \frac{\lambda}{\Delta\lambda} = mN, \quad (10)$$

where λ is the wavelength of light, $\Delta\lambda$ is the smallest resolv-

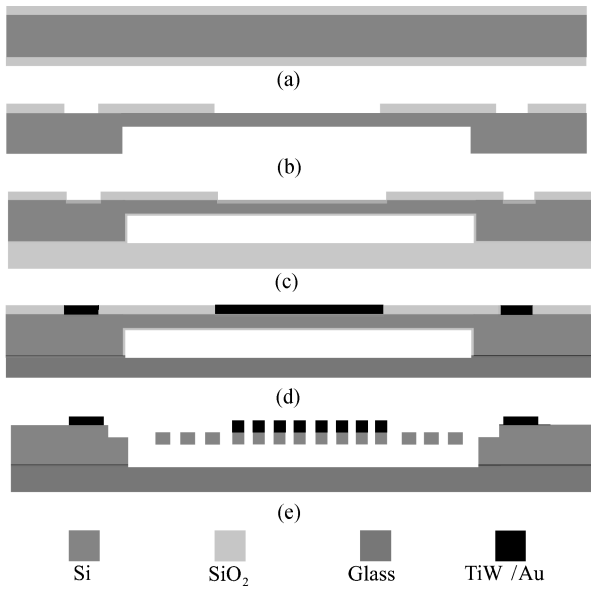


Fig. 4. Fabrication processes of the tunable MEMS grating.

able wavelength difference, m is the diffraction order, and N is the number of grating slats. Equation (10) shows that the diffraction resolving power is also improved by a small grating period. Also, the duty cycle of the grating device increases with decreasing grating period, which leads to an improvement in the diffraction efficiency. As a result, the compressed structure can reduce the grating period with tuning and enlarge the diffraction angle, improve the grating diffraction efficiency and resolution. Secondly, the initial period does not need to be very small in order to achieve a similar performance. Consequently it will simplify the fabrication process and improve the yield. Furthermore, the designed structure is symmetric about both the x -axis and y -axis to keep the grating moving in the lateral direction.

3. Fabrication

The process flow is shown in Fig. 4. It started from a normal 4-inch silicon wafer with 300 μm thickness. After the first thermal oxidization of 500 nm (a), the wafer was patterned and etched for 250 μm thick silicon on the backside with deep reactive ion etching (DRIE) (b), leaving a silicon layer of 50 μm as the movable structure layer. After another thermal oxidization of 200 nm, the wafer was bonded to glass at vacuum (c). Then, a 300 nm thick Au was sputtered to the grating to increase the diffraction efficiency and form the metal contact (d). After patterning and etching the metal and silicon dioxide by ion beam etching and following a DRIE of 50 μm thick silicon, the wafer was dipped into a buffered HF acid and released by a CO_2 supercritical desiccation to prevent it from cracking and sticking to the substrate (e). The minimum feature was 2.5 μm .

A typical aspect of the device can be found in Fig. 5. Figure 5(a) shows the entire device. Figure 5(b) shows the details of the comb drivers and the tilted folded beams. Figure 5(c) shows close-up views of the grating slats and the spring flexures. As presented in the figures, the frame of the device is hollowed out to lighten the weight of the device.

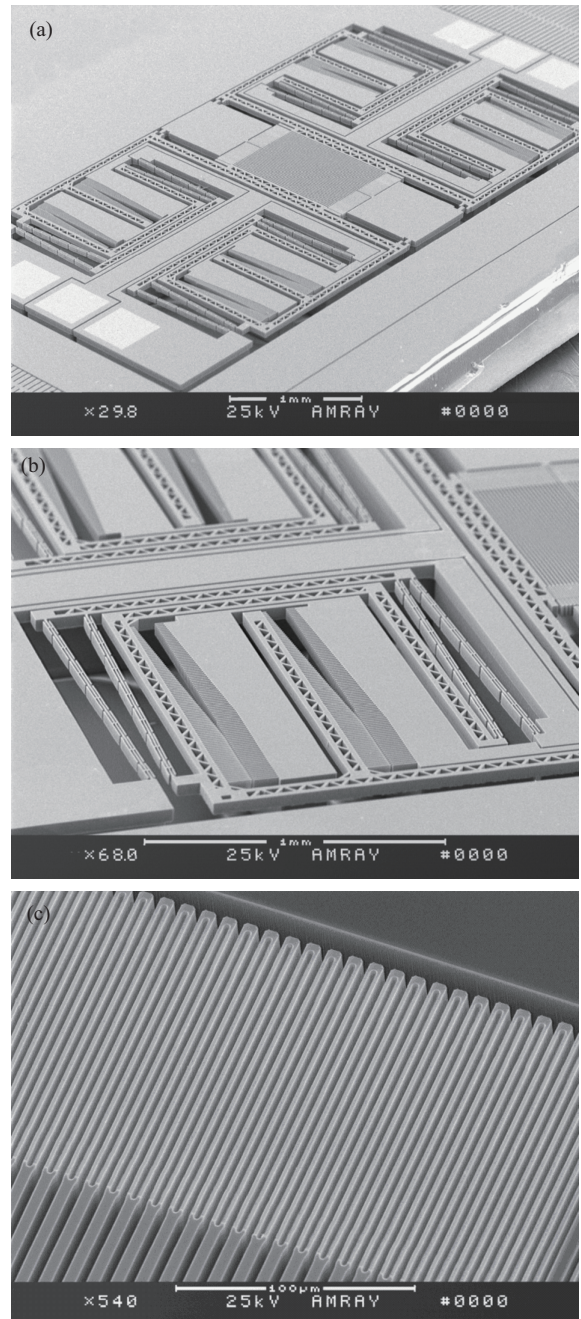


Fig. 5. SEM images of the compressed tunable grating. (a) Entire device. (b) Comb drivers and tilted folded beams. (c) Grating slats and spring flexures.

4. Characterization

4.1. Mechanical characterization

The grating device is connected to a printed circuit board (PCB) with wire bonding for testing. With the help of a high-resolution measuring microscope Hirox KH-7700, the relationship of the grating displacement to the applied voltage was measured. Figure 6 shows the measured displacement versus the applied voltage. It demonstrates that under a voltage of 37 V, each end of the grating device can be compressed by 72 μm , and the whole grating device with 71 movable grating slats can be compressed by 144 μm . This indicates that each

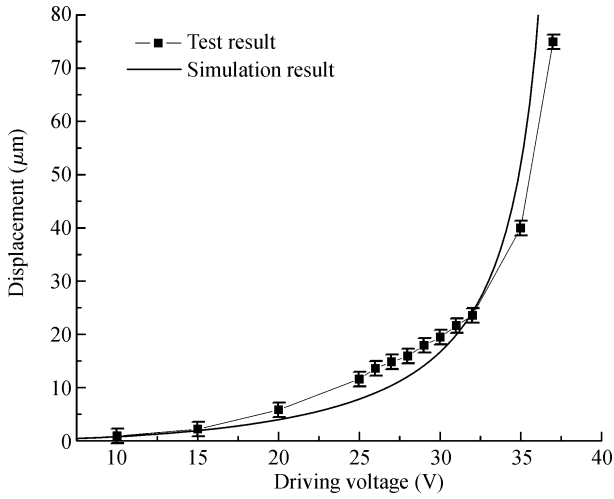


Fig. 6. Applied voltage versus the measured (black dots) and simulated (solid line) displacement for the 16 μm period grating.

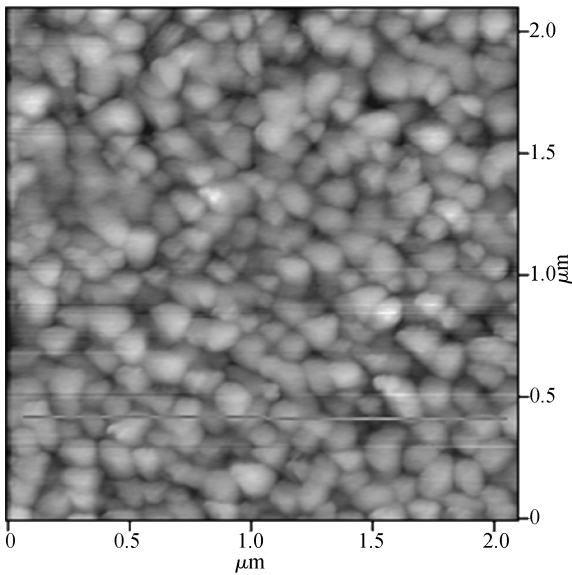


Fig. 7. AFM image of the grating.

grating is compressed by 2 μm and the relative tuning of the grating period $\Delta\lambda/\lambda$ is 12.5%. The comb drivers are unstable and are pulled in when the applied voltage increases to 38 V.

The simulation results are also shown in Fig. 6. They indicate that the simulation results and test results are in good agreement when the displacement is small. However, there are distinct differences with large displacement. These originate from the nonlinearity of the beam at large displacement and the process tolerance.

4.2. Optical characterization

A gold layer is sputtered to the grating to increase the diffraction efficiency. Figure 7 shows the AFM view of the grating after the whole process is completed. It indicates that the root-mean-square roughness of the grating surface is only 2.764 nm and the sputtered gold film has a good profile, which means that the fabrication processes have little effect on the gold surface profile. The measured reflectivity using an FTIR

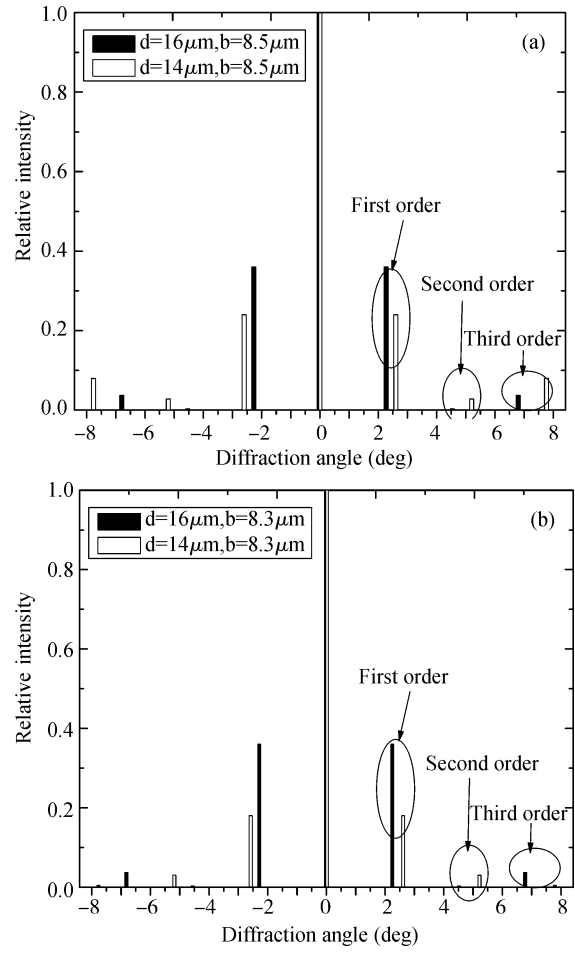


Fig. 8. (a) Simulated and (b) measured results of the grating diffraction intensity with a He-Ne laser at 632.8 nm before (solid bar) and after (blank bar) tuning the grating period (16 μm to 14 μm).

spectrometer (Bruker, Vertex 70v) is more than 92.6% in the wavelength region from 2.5 to 10 μm.

The optical behavior of the grating was characterized by a He-Ne laser at 632.8 nm in static mode. The tested grating slat was 1000 μm long and 8.5 μm wide, and the slat gap was 7.5 μm, resulting in a period of 16 μm. The test results show that the maximum tuning range of the first order diffraction angle is 0.34° at 632.8 nm. In Fig. 8, the solid bar shows the intensity of the grating with the period of 16 μm before compressed, while the blank bar shows the intensity of the same grating with the period compressed to 14 μm. The difference in width of the grating slat between simulated data (Fig. 8(a), b = 8.5 μm) and measured data (Fig. 8(b), b = 8.3 μm) results from the tolerance of the fabrication process. As shown in Fig. 8, the experimental results of the grating diffraction intensity coincide well with the simulation results.

5. Conclusion

The design, fabrication and characterization of a MEMS compressed period-tunable grating with a wide tuning range and a continuously adjusting function are reported in this paper. The compressed structure is used to improve the performance, avoid the small initial period, and simplify the fabrication process. To achieve large tuning range and high speed,

comb driver actuators are employed. Eight developed comb actuators with small comb gap are adopted to increase the actuating force and decrease the working voltage. The comb actuators with non-initial comb overlap and linearly engaging comb fingers and tilted folded beams are employed to improve the side stability. According to the measurement results, a grating with a period of $16\ \mu\text{m}$ can be compressed laterally by $144\ \mu\text{m}$ under an applied voltage of $37\ \text{V}$, resulting in a grating period tuning of 12.5%. Our design decreases the driving voltage and greatly extends the tuning range. The optical characterization of the grating demonstrates that the maximum tuning range of the first order diffraction angle is 0.34° at $632.8\ \text{nm}$, which shows good agreement with the optical simulation result. The grating device can be fabricated with good yield by simple processes, and it can find promising applications in mid-infrared spectrometers.

References

- [1] Brazas J C, Kowarz M W. High-resolution laser-projection display system using a grating electromechanical system (GEMS). *Proc SPIE MOEMS Display and Imaging Systems II*, 2004, 5348: 65
- [2] Trisnadi J I, Carlisle C B, Monteverde R. Overview and applications of grating-light-valve-based optical write engines for high-speed digital imaging. *Proc SPIE MOEMS Display and Imaging Systems II*, 2004, 5348: 52
- [3] Kenda A, Scherf W, Hauser R, et al. A compact spectrometer based on a micromachined torsional mirror device. *Proc IEEE Sensors*, 2004, 3:1312
- [4] Wong C W, Kim S G. Analog piezoelectric-driven tunable gratings with nanometer resolution. *J Microelectromech Syst*, 2004, 13(6): 998
- [5] Shih W C, Kim S G. High-resolution electrostatic analog tunable grating with a single-mask fabrication process. *J Microelectromech Syst*, 2006, 15: 763
- [6] Tormen M, Peter Y A, Niedermann P, et al. Deformable MEMS grating for wide tunability and high operating speed. *J Opt A*, 2006, 8: S337
- [7] Aschwanden M, Beck M, Stemmer A. Diffractive transmission grating tuned by dielectric elastomer actuator. *IEEE Photonics Technol Lett*, 2007, 19: 1090
- [8] Yang Y S, Lin Y H, Hu Y C, et al. A large-displacement thermal actuator designed for MEMS pitch-tunable grating. *J Micromech Microeng*, 2009, 19: 015001
- [9] Tang W C, Nguyen T H, Howe R T. Laterally driven polysilicon resonant microstructures. *Sensors Actuators*, 1989, 20: 25
- [10] Legtenberg R, Groeneveld A W, Elwenspoek M. Comb-drive actuators for large displacements. *J Micromech Microeng*, 1996, 6: 320
- [11] Grade J D, Jerman H, Kenny T W. Design of large deflection electrostatic actuators. *J Microelectromech Syst*, 2003, 12: 335
- [12] Ming A, Li T, Zhou P, et al. An electrostatic MEMS actuator with large displacement under low driving voltage. *Journal of Semiconductors*, 2008, 29: 1703
- [13] Zhou G, Dowd P. Tilted folded-beam suspension for extending the stable travel range of comb-drive actuators. *J Micromech Microeng*, 2003, 13: 178
- [14] Liu X, Li T, Ming A, et al. MEMS compressed tunable grating. *Proc SPIE International Symposium on Photoelectronic Detection and Imaging*, 2009, 7381: 73812L